

Generation of multiple-charged optical vortex solitons in a saturable nonlinear medium

A. Dreischuh,* G. G. Paulus, F. Zacher, F. Grasbon, and H. Walther
Max-Planck-Institut für Quantenoptik, Hans-Kopfermann-Straße 1, 85748 Garching, Germany
 (Received 4 December 1998)

Multiply charged optical vortex solitons (OVS) ($m = 1, \dots, 4$) are generated in a thermal nonlinear medium with saturation. The respective soliton constants are found to be linearly proportional to the topological charges. Special attention is paid to the modulational instability, which is effectively suppressed by a moderate saturation but still remains an increasing function of the topological charge. For the particular experimental conditions, the recorded OVS profiles are found to be in good qualitative agreement with the numerical stationary solutions of the generalized nonlinear Schrödinger equation. [S1063-651X(99)17910-8]

PACS number(s): 42.65.Tg, 42.65.Sf

I. INTRODUCTION

In the past, the considerable theoretical and experimental interest in the optical dark spatial solitons (DSSs) was inspired not only by the intriguing physical picture presented [1], but also by the possible applications in all-optical guiding and switching devices [2,3]. The only known truly two-dimensional (2D) DSSs are the optical vortex solitons (OVSs) [4]. They are characterized as localized self-supporting intensity dips with screw phase dislocations imposed on bright background beams. In self-defocusing nonlinear media (NLM), such solitons are generated as a result of the balance between diffraction and nonlinearity [4]. The characteristic helical phase profile is analytically described by an $\exp(im\varphi)$ multiplier, where φ is the azimuthal coordinate and the integer number m is the so-called topological charge (TC).

As compared to the singly charged OVSs, those with TCs $|m| > 1$ have seen less theoretical investigation [5,6]. This is due in part to the vortex dynamics of the nonlinear wave equation. A vortex of charge $|m| \geq 2$ is found to be topologically unstable against bifurcation into $|m|$ branches [7]. Multiply charged quantum vortices are also expected to be unstable, since the free energy scales with m^2 [8]. However, the nonlinear Schrödinger equation (NLSE) can be considered as a special kind of Ginzburg-Landau equation for which multiply charged vortices may be stable in a certain range of parameters [9]. The saturation of the third-order nonlinearity involved in the generalized NLSE is proven to suppress effectively the DSS transverse instability [10]. The latter inspired this first experimental study of the generation and stability of OVSs with topological charges $m = 2, \dots, 4$ in a saturable self-defocusing nonlinear medium. Special attention has been paid to clearly distinguishing the formation of metastable self-supported dark beams and their instability decay. The sensitivity of the OVSs to perturbations is found to increase with m . The data presented confirm quantitatively the prediction [11] that the OVS constant grows linearly with the TC. For these particular experimental condi-

tions, the transverse profiles of the generated m -fold charged OVSs are found to be in good qualitative agreement with the stationary solutions of the 2D NLSE [6].

II. EXPERIMENT SETUP

The first step in this experiment was to evaluate the quality of the OV beams used. These are created by illuminating photolithographically fabricated computer-generated holograms (CGHs) [12,13] with an Ar⁺-ion laser ($\lambda = 488$ nm). The binary type CGHs are produced on a common substrate at a grating period of 20 μm with a cross section of 5×5 mm². The diffraction efficiency at first order is measured to be 9%, close to the theoretical 10% limit [12] for holograms of this type. Within the CGHs, it is easy to recognize the center of the m -fold charged vortex beam by the converging of m neighboring lines in one. Making use of the four-frame technique for interferogram analysis [14,15], we reconstructed the phase distributions of the OV beams. The method requires recording a set of (four) interference pictures at known phase shifts. Interference pictures are obtained by gently focusing the first diffraction order beam and passing it through the object arm of an asymmetrical Mach-Zehnder interferometer [Fig. 1(a)]. The zero diffraction order beam passes its reference arm. Controllable phase shifts in this arm are introduced by rotating a pair of 5 mm quartz substrates in opposite directions. Each interference pattern is projected directly onto a charge-coupled-device (CCD) camera array of 13 μm resolution and stored in a personal computer by an image-capturing card. In Fig. 2 we present the two-dimensional phase distributions for OV beams with charges $m = 1$ (a) and $m = 2$ (b). As pointed out in [13], a clear signature for the presence of a phase singularity is a new fringe starting at the location of the singularity. The vertical diametric phase distribution of the singly charged OV extracted from this phase portrait [Fig. 2(a)] is shown in Fig. 3. The deviation of the phase jump from the required value of π is estimated to be approximately $\pi/20$. This is in reasonable agreement with the unavoidable quantization inaccuracy of $\pi/24$ for binary CGHs [14]. At a distance of 120 cm behind the hologram, the typical inaccuracy in localizing the position of the dislocation increases from 40 to 75 μm for $m = 1$ and $m = 3, 4$, respectively. This effect is caused, at least partially, by the larger widths of the dark OV beams with higher TCs (Fig. 4; see also [7,11]) and by the associated reduction of the interference pattern visibility at the dark

*Permanent address: Department of Quantum Electronics, Sofia University, 5 J. Bourchier Blvd., 1164 Sofia, Bulgaria. FAX: +3592/9625276. Electronic address: ald@phys.uni-sofia.bg

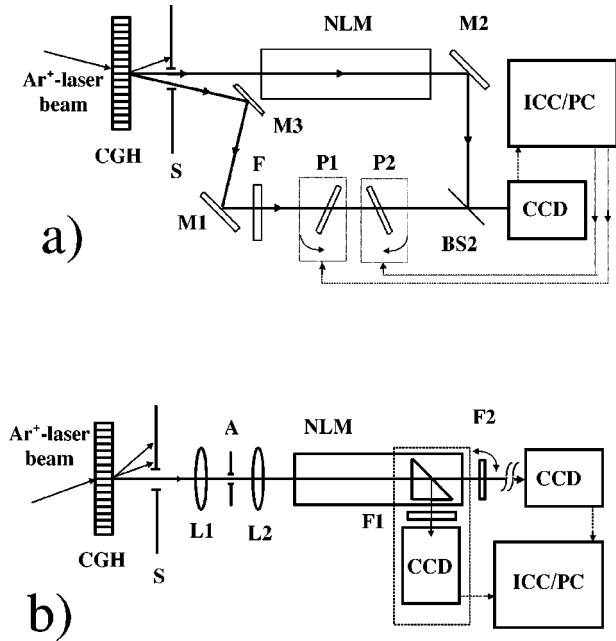


FIG. 1. Experimental arrangements used to obtain the two-dimensional phase distribution of OV beams of charges m (a) and to study their evolution along the thermal nonlinear medium (b). (CGH, computer-generated hologram; S, slit; BS1,BS2, beam splitters; M1,M2, mirrors; P1,P2, 5 mm thick plane-parallel quartz plates; L1,L2, AR-coated lenses ($f=80$ mm); A, iris aperture; F1,F2, filter sets; CCD, charge-coupled-device camera with $13 \mu\text{m}$ resolution; PC/ICC, personal computer equipped with an image capturing card).

beam axis. The intensity distributions are obtained on a screen placed 3.5 m behind the holograms (and after passing the beam through the NLM) at an input power of 5 mW. In view of the data presented in the next section, these radial intensity profiles should be considered as far-field and linear ones. The ratio of the background beam radius r_{BG} to the OV beam radius r_{OV} [both measured as half widths at half maximum (HWHM)], at the entrance window of the cell is estimated to be $r_{BG}/r_{OV}=20, 14, 12,$ and 11 for $|m|=1, 2, 3,$ and $4,$ respectively. Although the host beam cannot be considered to be an infinite one, it is wide enough to prevent the vortex-to-background interaction.

The experimental setup for investigating the OVS formation is shown in Fig. 1(b). The first-order background beam with the OV nested in it is transmitted through a slit placed some 15 cm behind the CGH and is subsequently focused on the entrance of the NLM. The nonlinear medium is ethylene glycol dyed with DODCI (Lambdachrome) to reach an absorption coefficient of $\alpha=0.107 \text{ cm}^{-1}$ at $\lambda=488 \text{ nm}$. After passing the desired nonlinear propagation path length, the dark beam is partially reflected by a prism that is immersed in the liquid to project the beam directly on a CCD array with a resolution of $13 \mu\text{m}$. Two filter sets ($F1$ and $F2$) are used to avoid saturation of the CCDs. The immersed prism, the filter set $F1$, and one of the cameras are mounted on a translation stage, enabling us to scan nonlinear propagation path lengths ranging from 0.5 to 8.5 cm. The filter set $F2$ is placed on a rotation stage and offers the possibility of recording unsaturated interference pictures after the maximal NLM length of 10 cm in this experiment (without prism im-

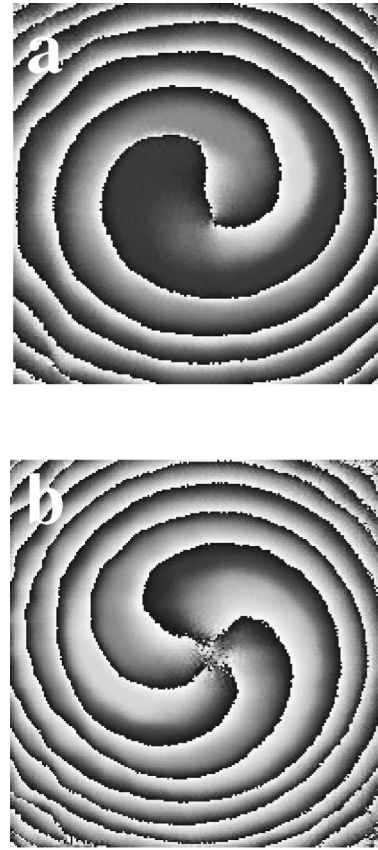


FIG. 2. Phase portraits of a singly charged (a) and doubly charged (b) OV beam obtained using the four-frame technique (see the text). Black and white denote phases of $-\pi/2$ and $\pi/2$, respectively.

mersed). The same camera is also utilized to monitor the far-field energy-density distribution and to identify the development of a modulational instability.

III. GENERATION OF OVVS

A. Singly charged OVS

The power dependence of the product of the peak dark irradiance and the square of the dark beam width (HWHM)

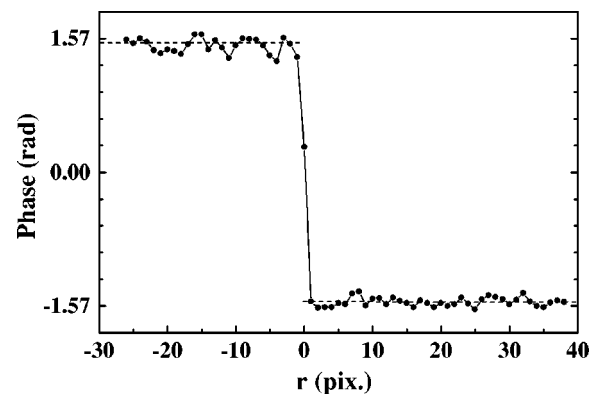


FIG. 3. Vertical diametrical phase distribution of a singly charged OV beam extracted from the experimental phase distribution shown in Fig. 2. Dashed lines: mean values of the phase outside the vortex core.

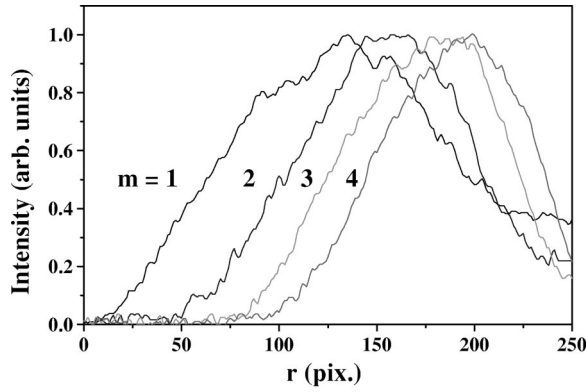


FIG. 4. Far-field radial intensity distribution of OV beams of topological charges $m=1, \dots, 4$ recorded at a distance of 3.5 m behind the CGHs.

Ia^2 for a singly charged OV beam is presented in Fig. 5. The data are recorded after a nonlinear propagation path length of 8 cm. In order to avoid the CCD-camera saturation, the filter set $F1$ [Fig. 1(b)] is changed at input powers of 17.5 and 47.5 mW. No change in the number of dark beams is observed at offsets of the dislocation with respect to the axis of the background. After correcting the experimental data for absorption and focusing, the stationary value of Ia^2 (Fig. 5, dashed line) is used as a reference in comparing the soliton constants of OVSs of charges $|m|=2, 3$, and 4 (Sec. III E).

B. Doubly charged OVS

The evolution of the incoming doubly charged OV beam with a power up to 70 mW is studied after a nonlinear propagation distance of 7 cm (Fig. 6). The filter set $F1$ is changed at 17.5, 47.5, and 57.5 mW. As in the previous case, the quantity Ia^2 saturates and reaches its asymptotically constant value (at $P \approx 45$ mW). Since OVSs with TCs higher than one are expected to be unstable against decay into singly charged ones [7–9,16], we carefully tried to minimize the aberrations introduced by the focusing system. Throughout this work, an intentional perturbation means an increase of the aberrations in the focusing system by horizontal misalignment of the lens $L2$ [Fig. 1(b)]. The reproducibility of this ‘‘perturba-

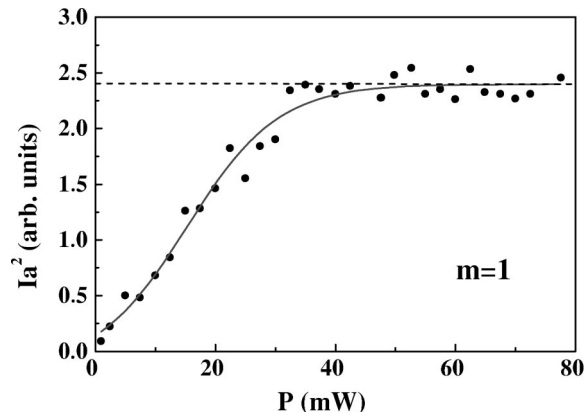


FIG. 5. Power dependence of the quantity Ia^2 for an OVS of a TC $|m|=1$ demonstrating saturation and stabilization. (Solid curve, best fit; dashed line, the soliton-constant value.)

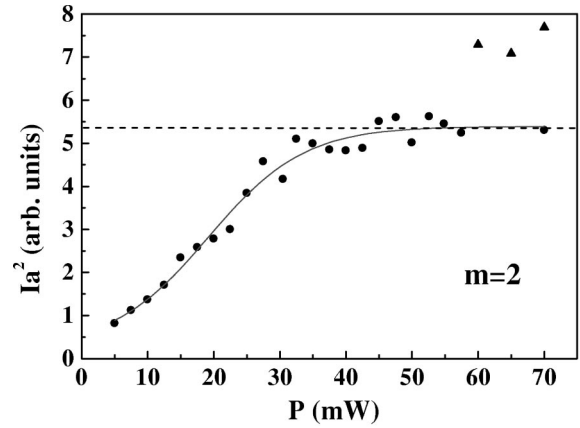


FIG. 6. Same as in Fig. 5 for $|m|=2$ at $z=7$ cm. (Circles, stable doubly charged OV beam; triangles, decay into singly charged OVSs.)

tion’’ is important for the subsequent comparison between the decay stages for the OV beams with different topological charges.

As a consequence of such a misalignment, we observed the creation of an elliptical dark beam for $|m|=2$. The quantity Ia^2 (measured along the longer axis) significantly deviates from the respective values at a careful alignment. The corresponding data are presented in Fig. 6 with solid triangles. The pronounced difference between the last two points obtained at 70 mW allows us to state that we are able to distinguish clearly between stable doubly charged OVSs (dots) and singly charged OV beams with overlapping cores (triangles). Complete separation between the vortices in the far field is not observed. In Fig. 7 we present two tracings of the interference patterns recorded at $z=7$ cm and an input power of $P=60$ mW. The decay of the doubly charged OVS [Fig. 7(a)] into two singly charged OVSs [Fig. 7(b)] is well pronounced. The separation between the axes of the screw dislocations after the decay is estimated to be approximately $160 \mu\text{m}$ [Fig. 7(b)].

C. Triple-charged OVS

Figure 8 represents the quantity Ia^2 vs input power P for an OV of charge $|m|=3$. The soliton constant is reached at higher powers (approximately 55 mW) as compared to the cases of $|m|=1$ and 2 and is accordingly higher. Unfortunately, the modulational sensitivity of the dark soliton is also higher. This can be easily recognized by considering Figs. 9(a) and 9(b). These interference images are recorded at a nonlinear propagation path length of 6 cm, at $P=72.5$ mW, and at equal but opposite offsets of the focusing lens $L2$



FIG. 7. Interference patterns (converted to black and white) corresponding to an OVS with a TC $|m|=2$ (a) and to two singly charged OVSs ($z=7$ cm, $P=60$ mW).

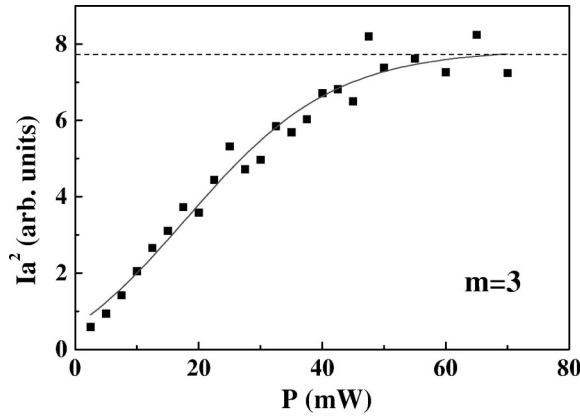


FIG. 8. Power dependence of the quantity Ia^2 for an OV beam of a charge $|m|=3$ obtained at $z=6$ cm. (Solid curve, best fit; dashed line, the respective soliton constant.)

[Fig. 1(b)] with respect to its correct position. The coexistence of displaced phase dislocations with TCs $|m|=2$ and $|m|=1$ is clearly seen. In our view, these images can be explained by the saturation of the nonlinearity, which is able to suppress effectively the DSS instability. As a result, the perturbation can appear to be critical for an OV beam with charge $|m|=3$ while remaining noncritical for singly and doubly charged OVSs. Our analysis carried out for Kerr NLM has shown [11] that multiply charged OVSs are always unstable and the critical wave number of the perturbation is proportional to $|m|$. In the experiment carried out under moderate saturation, the OVS modulational stability decreases with increasing TC but the highly charged OVSs are not necessarily unstable.

By keeping all conditions unchanged but increasing the input power up to 75 mW, we observed a complete decay of the intermediately stabilized formation [Fig. 9(b)] into three OVSs of TCs equal to one. The last results emphasize the significance of the saturation as a stabilization mechanism and provide motivation for its more precise quantitative estimation (see Sec. IV).

D. OVSs with charge $|m|=4$

The conclusions from Sec. III C are in agreement with the behavior of an OV beam with charge four. The measured soliton constant is higher as compared to this for $|m|=1, 2$, and 3 (Fig. 8). Assuming that an OVS is formed at an input power of 60 mW, the range corresponding to stable soliton formation extends over 15 mW only. At 80 mW input power

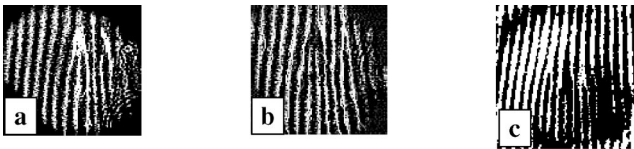


FIG. 9. Interference patterns (converted to black and white) corresponding to a triply charged OVS after a decay into doubly charged and singly charged OVS (a,b) and complete decay into three OVSs of charge $|m|=1$. Frames (a) and (b) refer to symmetrical opposite intentional perturbations at $P=72.5$ mW, whereas frame (c) is recorded at 75 mW.

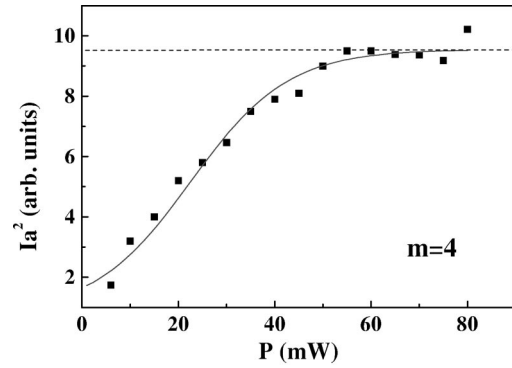


FIG. 10. Same as in Fig. 8 for an OVS of charge $|m|=4$. The nonlinear propagation path length is $z=5.5$ cm.

we do not observe stable four-times-charged OVSs with axial symmetry (see the last point in Fig. 10). The intentional perturbation is found to cause a complete decay of the dark beam into four singly charged OVSs. The latter is clearly seen from the interference pattern in Figs. 11. Since the input power is kept constant (80 mW) the rotation of the ordered structure of charge-one OVSs is due to the increase in the nonlinear propagation path length [17,18] [$z=6.5$ cm for Fig. 11(a) and $z=7.5$ cm for Fig. 11(b)]. The rotation angle is found to depend strongly (within $\pm 15\%$) on the perturbation strength. This should be attributed to the different initial instability growth rates. The decay into a line of OVSs instead, for instance, in a rectangular structure, is due to the lens misalignment along a single axis.

E. Evaluation of the soliton constants

By keeping the background beam power/intensity unchanged and translating the prism immersed in the NLM, we obtained the dependencies of the OV beam radii $r_{OV(m)}$ on the nonlinear propagation path length z (Fig. 12) for different TCs. Our starting hypothesis [11] (well motivated by Figs. 5, 6, 8, and 10) is that the soliton constant of an m -fold-charged OVS equals $|m|$ times the soliton constant of a singly charged OVS. In other words, in the absence of absorption and focusing,

$$I_{BG} r_{OV(m)}^2 = |m| C. \quad (3.1)$$

Including focusing [19,20] and absorption, Eq. (1) becomes

$$\frac{I_{BG}(z=0)e^{(-\alpha z)}}{[1 + (z/L_{diff})^2]} r_{OV(m)}^2(z=0)e^{2\beta z} = |m| C, \quad (3.2)$$

where L_{diff} is the Rayleigh diffraction length of the core, α is the linear absorption coefficient ($\alpha=0.107$ cm $^{-1}$), and β



FIG. 11. Gray-scale images of a decayed four-times-charged OVS. The images in (a) and (b) are recorded at $P=80$ mW and $z=6.5$ and 7.5 cm, respectively.

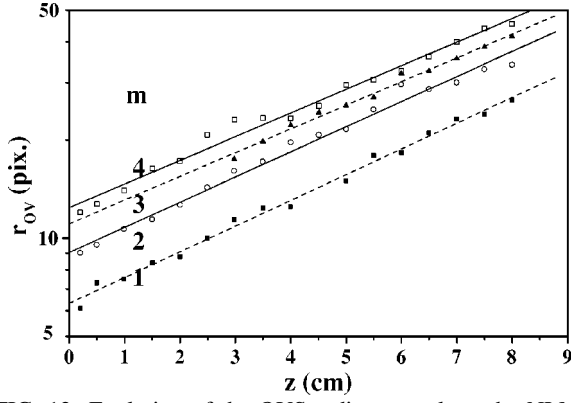


FIG. 12. Evolution of the OVS radius r_{OV} along the NLM for different values of the topological charge m (see the text).

is the only fitting parameter reflecting the increase in $r_{OV(m)}$ vs z . If the formulated hypothesis [Eq. (1)] holds exactly, the parameter β extracted from the curves in Fig. 12 should satisfy the relation

$$\exp(2\beta - \alpha)z = 1 + (z/L_{diff})^2. \quad (3.3)$$

In Table I we summarize the estimated values of β and L_{diff} for OVSs with charge $|m|$, as well as the reverse calculated [by Eq. (2)] topological charges m' . The perfect agreement between the TCs encoded in the holograms and those recalculated for the respective OVSs provides strong evidence of the linear proportionality of the soliton constants to the charges.

IV. INFLUENCE OF THE SATURATION

Two particular aspects of the nonlinearity saturation are of special importance in this work, namely, the effective stabilization of the OVSs of charge $|m| > 1$ (see, for example, Fig. 9) and the reshaping of the corresponding intensity profiles (Figs. 4, 14). In the case of a local nonlinear response, the theory of the OVSs in strongly saturable media was recently developed [6]. Using this theory at the end of this section, we will present a qualitative picture of the influence of the nonlocality on the OVS intensity profiles.

Two independent measurements are carried out in order to estimate quantitatively the saturation intensity I_{sat} . In the first one we intentionally tilted the prism immersed in the NLM. In this way we realized a self-bending scheme similar to that used by Kaplan [21] and by Borodin and Kamuz [22]. The only difference lies in the symmetry of the incoming background beam with the OV nested. The asymmetry required is introduced by the different nonlinear propagation

TABLE I. Encoded in the CGHs and recalculated [by Eq. (3.2)] topological charges m and m' of the OVSs generated. The values of β and L_{diff} are extracted from Fig. 12 and from an independent measurement in a linear regime.

m	2β (cm $^{-1}$)	L_{diff} (cm)	m'
1	0.36(5)	2.5	1[$\pm 0.04(5)$]
2	0.35	3.2	2(± 0.08)
3	0.35	3.2	3(± 0.05)
4	0.33	3.1	4(± 0.01)

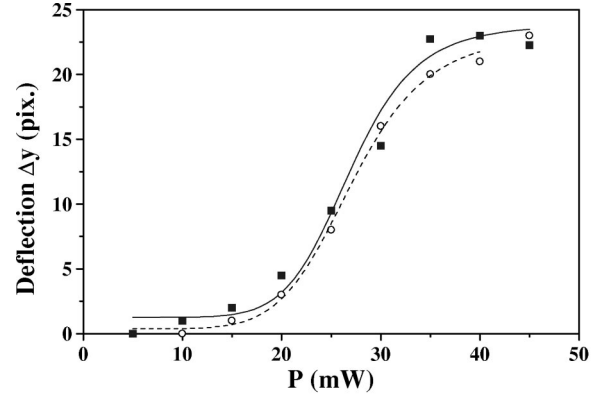


FIG. 13. Self-bending Δy of the background beam (circles; $z = 1.5$ cm) due to the tilt of the prism immersed in the NLM [see Fig. 1(b)] and near-field self-deflection of a half cut laser beam (squares; prism absent, $z = 10$ cm) vs input power. Solid and dashed lines: best sigmoidal fits of the type $\Delta y \sim I/(1+I/I_{sat})^3$.

length of the particular beam parts due to the prism tilt. The strength of the self-bending effect vs input power/intensity is measured by the change of the near-field position of the OV (Fig. 13, circles). In the absence of saturation the deflection Δy should remain proportional to the intensity I . The data, however, demonstrate well pronounced saturation. Since the choice of a suitable saturation model for an absorptive non-local nonlinearity is not trivial [23], we tried to find a best fit to the experimental data. A sigmoidal one of the type $\Delta y \sim I/(1+I/I_{sat})^\gamma$ enabled us to estimate $P_{sat} = 29$ mW at $\gamma = 3$.

In an independent measurement, we removed the CGH and the prism [see Fig. 1(b)]. The laser beam was half cut by a knife edge and imaged near the entrance window of the quivette. The same scheme was used by Swartzlander, Yin, and Kaplan to study the self-bending effect in metal vapors [24] and in experiments on dark spatial soliton formation [25]. The best sigmoidal fit yields $P_{sat} = 27$ mW at $\gamma = 3$. It is worth noting that by neglecting the first three experimental points corresponding to an effective onset of the nonlinearity, the fitting model used in [23] under substantially different conditions gives practically the same values of P_{sat} with an accuracy of ± 1 mW. In the rest of this work the saturation parameter s refers to $P_{sat} = 28$ mW. From the data we estimated (see also [24]) the maximal nonlinear correction to the medium refractive index reached $\Delta n_{max} = 10^{-3}$ ($\pm 15\%$).

The quantitative estimation of the saturation parameter s was necessary to model the stationary OVS profiles at the particular experimental conditions. We used the stationary NLSE that is correctly derived for refractive-index saturation corresponding to the standard two-level model [6]. We found a formal motivation for this in the coincidence between the values of P_{sat} derived by the different saturation models. In this way, however, the nonlocality of the NLM remains completely neglected.

In Fig. 14 we present a comparison between calculated unsaturated (solid curves) and saturated (dashed curves) radial electric field distributions of OVSs of TCs $m = 1, \dots, 4$. As seen, the general tendency of increasing OVS radii with increased TCs is clearly expressed in both cases with and without saturation. The results agree well with the conclusion [6] that at a fixed TC the size of the vortex core is highly sensitive to variations of the dimensionless saturation

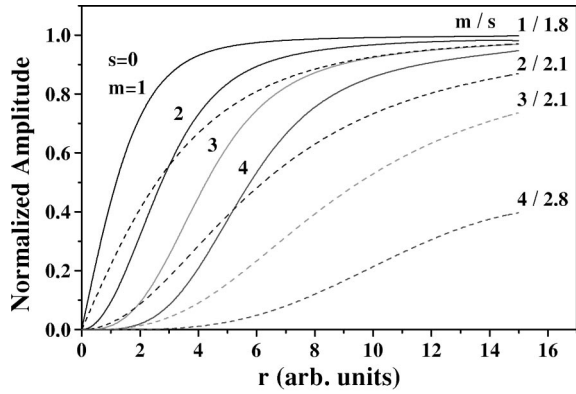


FIG. 14. Stationary localized solutions of the NLSE: Solid curves, radial field distributions of OVSs of topological charges $m=1-4$ in the absence of nonlinearity saturation ($s=0$); dashed curves, the same but at saturation levels $s=I/I_{sat}$, corresponding to the particular experimental conditions under which the multiply charged OVSs are generated (see text).

s . In that sense the comparison of the numerical data with the experimental ones is highly desirable. Figure 15(a) shows the measured radial intensity profiles of OVSs with charges $m=1$ and 2 (circles and triangles, respectively) and the corresponding numerical results (solid curves, see also Fig. 14) at the particular saturation levels. Figure 15(b) presents the same data for OVSs of charges $m=3$ and 4 (denoted with diamonds and squares, respectively). The tendency toward OVS core radii increasing with increasing TCs is very pronounced, but the difference between the experimental and numerical data is quite large at low TCs [Fig. 15(a)]. For $m=3$ the agreement becomes reasonable and for $m=4$ seems to be quantitatively good [Fig. 15(b)]. Since an underestimation of the saturation is not likely, the differences should be attributed to the nonlocality of the thermal nonlinearity. Its influence seems to be negligible only on a spatial scale of more than $500 \mu\text{m}$.

V. CONCLUSION

In this work we presented experimental evidence of the existence of multiply charged OVSs modulationally stabilized by saturation of the nonlinearity. Unfortunately, this mechanism is not known to be able to remove the topological instability; however, it reduces the respective instability growth rates. In view of that, the OVSs generated should be classified as metastable. As expected ([11]) the OV soliton constants are found to be linearly proportional to the topological charges. As a result of an intentional perturbation, we observed incomplete decay of triply charged OV into doubly and singly charged OVSs. This confirms the effective suppression of the instability at (moderate) saturation [10]. In qualitative agreement with the preceding results for pairs of charge-one OVSs [17,18,20], complete decay of a four-

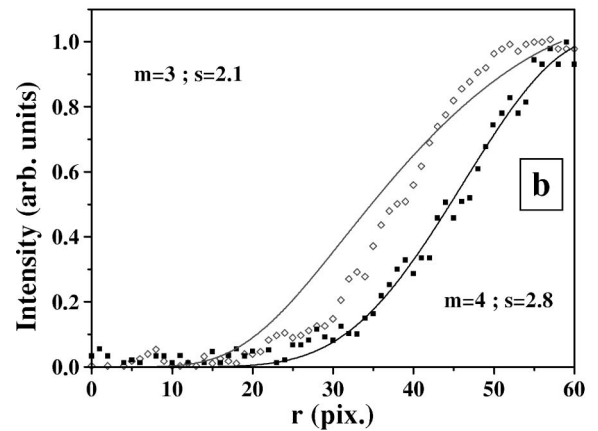
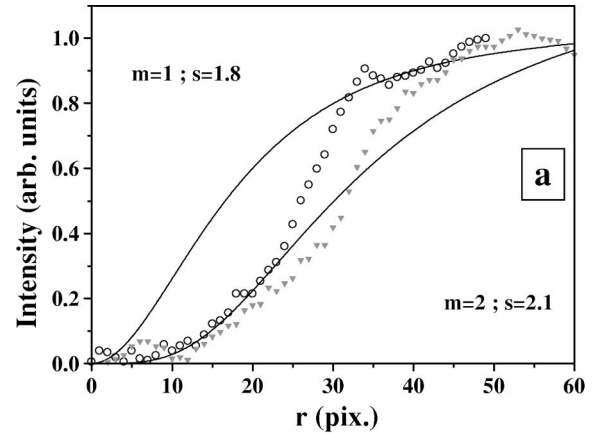


FIG. 15. Comparison between the stationary solutions of the NLSE under saturation and the experimentally obtained intensity profiles for OVSs of charges m under both saturation and nonlinearity nonlocality. (a) $m=1$ and 2 (circles and triangles); (b) $m=3$ and 4 (diamonds and squares); $s=I/I_{sat}$; solid curves show numerical results).

times-charged OV beam into a linear structure of four singly charged OVSs, as well as a rotation of the ensemble along the NLM, is observed. The quantitative estimation of the saturation power/intensity allows for a comparison between the theoretical (see [6]) and experimental radial OVS profiles. On this basis, the influence of the NLM nonlocality is discussed quantitatively.

ACKNOWLEDGMENTS

A.D. would like to thank the Alexander von Humboldt Foundation for their financial support and for the opportunity to work in the stimulating atmosphere of the Max-Planck-Institut für Quantenoptik (Garching, Germany). This work was also supported by the Science Foundation of Sofia University (Sofia, Bulgaria).

- [1] Yu. S. Kivshar and B. Luther-Davies, Phys. Rep. **289**, 81 (1997), and references therein.
 [2] B. Luther-Davies, and Y. Xiaoping, Opt. Lett. **17**, 496 (1992); **17**, 1755 (1992).

- [3] Z. Cheng, M. Shih, M. Segev, D. Wilson, R. Muller, and P. Maker, Opt. Lett. **22**, 1751 (1997).
 [4] G. A. Swartzlander, Jr., and C. T. Law, Phys. Rev. Lett. **69**, 2503 (1992); C. T. Law, and G. A. Swartzlander, Jr., Opt. Lett.

- 18**, 586 (1993).
- [5] D. Rozas, C. T. Law, and G. A. Swartzlander, Jr., *J. Opt. Soc. Am. B* **14**, 3054 (1997).
- [6] V. Tikhonenko, Yu. S. Kivshar, V. Steblina, and A. Zozulya, *J. Opt. Soc. Am. B* **15**, 79 (1998).
- [7] J. C. Neu, *Physica D* **43**, 385 (1990); **43**, 407 (1990).
- [8] R. J. Creswick, and H. L. Morrison, *Phys. Lett.* **76**, 267 (1980).
- [9] I. S. Aranson, K. A. Gorshkov, A. S. Lomov, and M. I. Rabinovich, *Physica D* **43**, 435 (1990).
- [10] B. Luther-Davies, J. Christou, V. Tikhonenko, and Yu. S. Kivshar, *J. Opt. Soc. Am. B* **14**, 3045 (1997).
- [11] I. Velchev, A. Dreischuh, D. Neshev, and S. Dinev, *Opt. Commun.* **140**, 77 (1997).
- [12] W.-H. Lee, *Prog. Opt.* **XVI**, 119 (1978).
- [13] N. R. Heckenberg, R. McDuff, C. P. Smith, and A. G. Wite, *Opt. Lett.* **17**, 221 (1992).
- [14] C. Creath, in *Holographic Interferometry*, edited by P. Rastogi (Springer-Verlag, Berlin, 1994), pp. 108–148; Th. Kreis, *Holographic Interferometry: Principles and Methods* (Academie-Verlag, Berlin, 1996), Chap. 4, pp. 123–139.
- [15] A. Dreischuh, W. Fließner, I. Velchev, S. Dinev, and L. Windholz, *Appl. Phys. B* **62**, 139 (1996); D. Neshev, A. Dreischuh, V. Kamenov, I. Stefanov, S. Dinev, W. Fließner, and L. Windholz, *ibid.* **64**, 429 (1997).
- [16] A. V. Mamaev, M. Saffman, and A. A. Zozulya, *Phys. Rev. Lett.* **78**, 2108 (1997).
- [17] B. Luther-Davies, R. Powles, and V. Tikhonenko, *Opt. Lett.* **19**, 1816 (1994).
- [18] D. Neshev, A. Dreischuh, M. Assa, and S. Dinev, *Opt. Commun.* **151**, 413 (1998).
- [19] V. Yu. Bazhenov, M. S. Soskin, and M. V. Vasnetsov, *J. Mod. Opt.* **39**, 985 (1992).
- [20] G. Indebetouw, *J. Mod. Opt.* **40**, 73 (1993).
- [21] A. E. Kaplan, *Pis'ma Zh. Eksp. Teor. Fiz.* **9**, 58 (1969) [*JETP Lett.* **9**, 33 (1969)].
- [22] M. S. Borodin and A. M. Kamuz, *Pis'ma Zh. Eksp. Teor. Fiz.* **9**, 577 (1969) [*JETP Lett.* **9**, 351 (1969)].
- [23] V. Tikhonenko, J. Christou, B. Luther-Davies, and Yu. S. Kivshar, *Opt. Lett.* **21**, 1129 (1996).
- [24] G. A. Swartzlander, Jr., H. Yin, and A. E. Kaplan, *Opt. Lett.* **13**, 1011 (1998).
- [25] G. A. Swartzlander, Jr., D. R. Andersen, J. J. Regan, H. Yin, and A. E. Kaplan, *Phys. Rev. Lett.* **66**, 1583 (1991).